RSC Advances

PAPER

View Article Online
View Journal | View Issue

Cite this: *RSC Adv.*, 2023, **13**, 20365

Gallium-based liquid metal hybridizing MoS_2 nanosheets with reversible rheological characteristics and enhanced lubrication properties

Xing Li, *[abc] Ruizhi Wang,[abc] Jiaqian Li,*[d] Guangneng Dong,[e] Qinghua Song,[ab] Bing Wang[ab] and Zhanqiang Liu[ab]

Received 6th April 2023
Accepted 13th June 2023

DOI: 10.1039/d3ra02297h

rsc.li/rsc-advances

Gallium-based liquid metal (GLM) is a promising lubricant candidate due to its high load capacity and high thermal stability. However, the lubrication performance of GLM is restricted by its metallic characteristics. Herein, this work proposes a facile method to obtain a GLM@MoS_2 composite by integrating GLM with MoS_2 nanosheets. The incorporation of MoS_2 imparts GLM with different rheological properties. Since GLM is able to be separated from the GLM@MoS_2 composite and agglomerates into bulk liquid metal again in alkaline solution, the bonding between GLM and MoS_2 nanosheets is reversible. Moreover, our frictional tests demonstrate that the GLM@MoS_2 composite exhibits enhanced tribological performance including reduction of friction coefficient and wear rate by 46% and 89%, respectively, in contrast to the pure GLM.

1. Introduction

Gallium-based liquid metal (GLM), such as eutectic Ga–In alloy or galinstan, has attracted significant attention for applications in composites[1–4] and also for their potential as novel lubricants.[5–8] GLM holds metallicity advantages including low melting point, low vapor pressure, low toxicity, good fluidity, high thermal stability, high thermal conductivity, and high extreme-pressure properties, which meet the requirements for extremely high temperature and pressure lubricants. However, the lubrication abilities of GLM are restricted by their metallic properties.[9] On account of high surface tension and chemically inertness, the anti-friction and anti-wear abilities of GLM is poor under low loads and speeds. The effective friction reaction films must be formed under extremely high friction work conditions. As a result, this metallicity–lubricity trade-off of GLM is limiting for emerging lubricant application.

In order to overcome this constraint, some efforts have been made to enhance the lubricity of GLM including optimizing the environmental atmospheres,[10] treating the surface texture of the frictional pairs[11] and modifying liquid metal with particles.[12,13] Among these efforts, modification liquid metal with specific micro and nano-particles is an effective and convenient method, which is suitable for most actual working conditions. There are mainly two methods to mingle functional particles into liquid metal alloy.[14–19] For metal particles, intermetallic wetting between liquid metal and particles can be induced by electrochemical reaction or acid solution. For non-metal particles, liquid metals' sticky oxides can be utilized to blend the particles by grinding or mechanical stirring. Guo *et al.* have reported that doping traces of aluminum element to GLM could enhance the lubricity of GLM.[12] However, metal particles hold a limited ability to improve the lubricity of liquid metal. And to date, the research about hybridizing non-metal particles into GLM for enhancing lubricity of GLM is relatively absent.

Some non-metal particles exhibit excellent lubrication ability such as MoS_2. MoS_2 is an inorganic compound with layered structure and the molecular force between layers is so weak that it is easy to slip between layers, resulting in low shear strength.[20,21] These characteristics impart good anti-friction effect to MoS_2, making it a widely used dry lubricant.[22,23] Furthermore, microscale or nanoscale MoS_2 have been proved to be a promising lubrication additive for both liquid and solid based lubricants with remarkable friction reduction and wear resistance performance.[24–27] For instance, Chacko *et al.* have reported that with appropriate concentrations of MoS_2 nanosheets, the lubrication behaviours of both coconut oil and paraffin oil could be enhanced.[28] Chen *et al.* have found that the addition of MoS_2 nanosheets was capable of improving the anti-friction and anti-wear properties of the bismaleimide resin.[29]

Herein, in present work, GLM@MoS_2 composite with desirable lubrication properties is designed by hybridizing MoS_2 nanosheets into GLM. GLM@MoS_2 composite is prepared by

[a]*School of Mechanical Engineering, Shandong University, Jinan, 250061, China. E-mail: xingli@sdu.edu.cn*

[b]*Key Laboratory of High Efficiency and Clean Mechanical Manufacture of MOE/National Demonstration Center for Experimental Mechanical Engineering Education at Shandong University, China*

[c]*Collaborative Innovation Center for Shandong's Main crop Production Equipment and Mechanization, China*

[d]*School of energy and power Engineering, Shandong University, Jinan, 250061, China. E-mail: jiaqianli@sdu.edu.cn*

[e]*Key Laboratory of Education Ministry for Modern Design and Rotor-Bearing System, School of Mechanical Engineering, Xi'an Jiaotong University, Xi'an 710049, China*

mechanical stirring and grinding, utilizing the sticky oxides of GLM. The bonding between GLM and MoS_2 nanosheets is reversible, which bestows reversible rheological characteristics on GLM@MoS_2 composite. In addition, the tribological tests prove that the prepared GLM@MoS_2 composite hold excellent lubrication properties.

2. Experiments

2.1 Materials

The GLM used in present work is $Ga_{76}In_{24}$ with a melting point at 16 °C and the preparation procedures of $Ga_{76}In_{24}$ are as the followings. First, Ga and In with mass ratio at 76 : 24 were mixed together in a graphite crucible. And then the mixtures were heated to the temperature of 180 °C under the vacuum condition for 30 minutes. After the heating treatment, a eutectic liquid metal alloy of Ga and In was produced. Finally, the eutectic liquid metal was ultrasonicated in a water bath for 15 minutes to promote the complete fusion of GLM. The densities of pure Ga and eutectic liquid metal, which are 6.1 g cm^{-3} and 6.8 g cm^{-3} respectively, which are in accordance with the previous studies.[30] MoS_2 nanosheets adopted in this work were purchased from Beijing Dk Nano technology Co., Ltd, China.

2.2 Preparation of GLM@MoS_2

GLM@MoS_2 was prepared by mechanical mixing and grinding methods and the detailed operational procedures were shown in Fig. 1. First of all, the GLM was added in a ceramic crucible. Once the GLM was exposed to air environment, the outer sphere of the GLM would oxide quickly and produce a nanoscale Ga_2O_3 film surrounding the GLM.[31] Then, MoS_2 nanosheets were placed in the crucible. As shown in Fig. 1a, MoS_2 nanosheets and GLM were separated by Ga_2O_3 layer. After that, pestle was utilized to grind the MoS_2 nanosheets into GLM for hours. The grinding process could break the Ga_2O_3 layers and the adhesion property of Ga_2O_3 could facilitate the dispersion of MoS_2 nanosheets in GLM.

2.3 Tribological experiments

The tribological tests were conducted utilizing a ball-on-disk tribometer (UMT-2, CETR Corporation Ltd, USA) in reciprocation friction mode. Experiments were performed at room temperature (25 °C) and ambient humidity (30 ± 2%). And the experimental time of each individual test was 30 min. The disk specimens are AISI52100 bearing steel disk with surface roughness of Ra 0.021 μm and the ball specimens are Φ9.5 mm AISI52100 steel with surface roughness of Ra 0.008 μm. The applied loads were set as 2, 5, 10, 15, 20, and 25 N and kept constant for each test. The sliding frequency was 2 Hz and the sliding stroke was 6 mm. GLM and GLM@MoS_2 were adopted as the lubricant. In order to ensure the repeatability of the results obtained, all tests were repeated three times. Before and after every individual test, the specimen was cleaned with ethanol in an ultrasonic bath for 15 minutes.

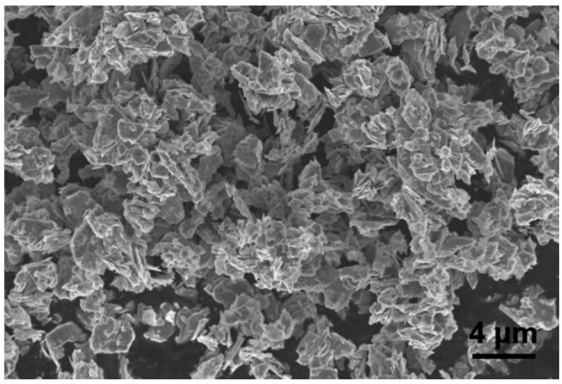

Fig. 2 SEM image of MoS_2 nanosheets adopted in this work.

Moreover, in order to specify the wear rate (k) for each experiment, we have calculated the wear volume (V) based on the corresponding wear scar radius of the ball through the following equations.

$$h = R - \sqrt{R^2 - r^2} \quad (1)$$

$$V = \pi \cdot h^2 \left(R - \frac{h}{3} \right) \quad (2)$$

$$k = \frac{V}{F \cdot S} \quad (3)$$

where h is the height of spherical cap, R is the original radius of the ball, F is the normal load in the experiment and S is the total sliding distance. For all experiments, we took three radii of each wear scar and calculated their average value.

2.4 Characterizations

Scanning electron microscopy (Gemini SEM 500, ZEISS, Germany) equipped with Energy dispersive spectrometer (EDS) was utilized to observe the morphology of GLM@MoS_2 composite

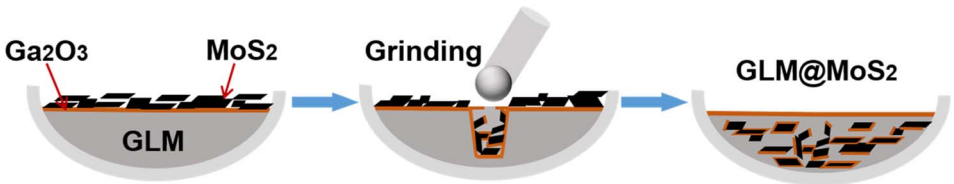

Fig. 1 Schematic presentation of preparation process of GLM@MoS_2. Initially, the GLM is surrounded by Ga_2O_3 oxides and separated from MoS_2 nanosheets. Then the grinding process make MoS_2 nanosheets disperse into GLM by the adhesion property of Ga_2O_3. And finally the GLM@MoS_2 composite is obtained.

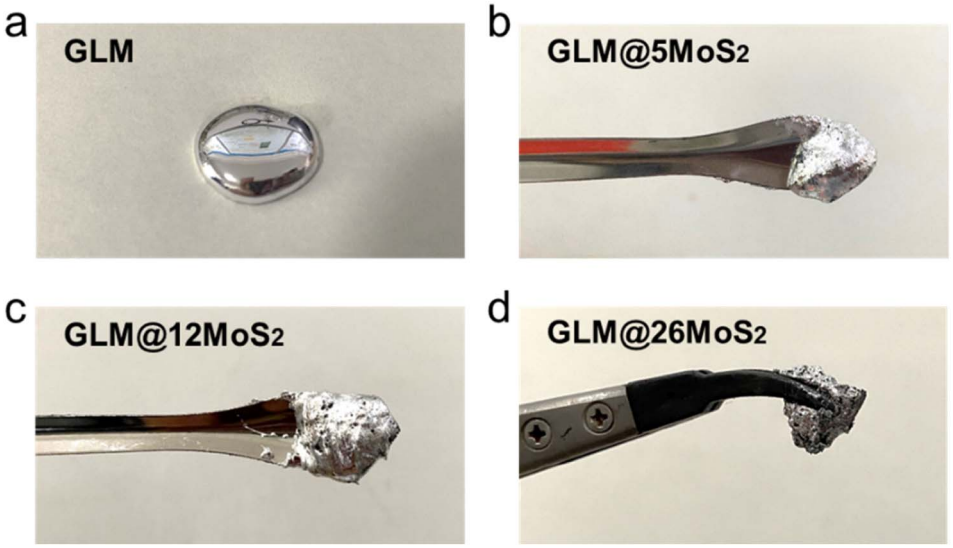

Fig. 3 (a) Image of pure GLM, (b) GLM with 5wt% MoS_2 nanosheets, (c) GLM with 12 wt% MoS_2 nanosheets, (d) GLM with 26 wt% MoS_2 nanosheets.

and MoS_2 nanosheets. Thermo gravimetric analyser (TGA) tests were conducted to evaluate the thermal properties of GLM@MoS_2 composite under an oxygen atmosphere from 30 to 800 °C (STA449C, NETZSCH, Germany). Optical microscope (OM) and SEM were used to observe the worn surfaces. EDS and X-ray photoelectron spectroscopy (XPS) were adopted to detect the chemical states of the worn tracks.

3. Results and discussion

3.1 The physical properties of GLM@MoS_2

The morphology of MoS_2 nanoparticles used in this work was characterized by SEM as shown in Fig. 2. The MoS_2 holds lamellar structure with the thickness less than 50 nm and the laminae size ranging from 1 μm to 3 μm. The appearance of pure GLM is a silver colour sheeny liquid as demonstrated in Fig. 3a. Different amounts of MoS_2 nanosheets were hybridized into GLM and the mass fractions of MoS_2 nanosheets in GLM were calculated by weighing the GLM with and without the MoS_2 nanosheets. The GLM with 5 wt%, 12 wt% and 26 wt% MoS_2 nanosheets are denoted as GLM@$5MoS_2$, GLM@$12MoS_2$ and GLM@$26MoS_2$. It can be seen from Fig. 3 that with the increase of MoS_2 nanosheets, the metallic luster of GLM@MoS_2 composite becomes darkened and the fluidity of GLM@MoS_2 composite becomes poor.

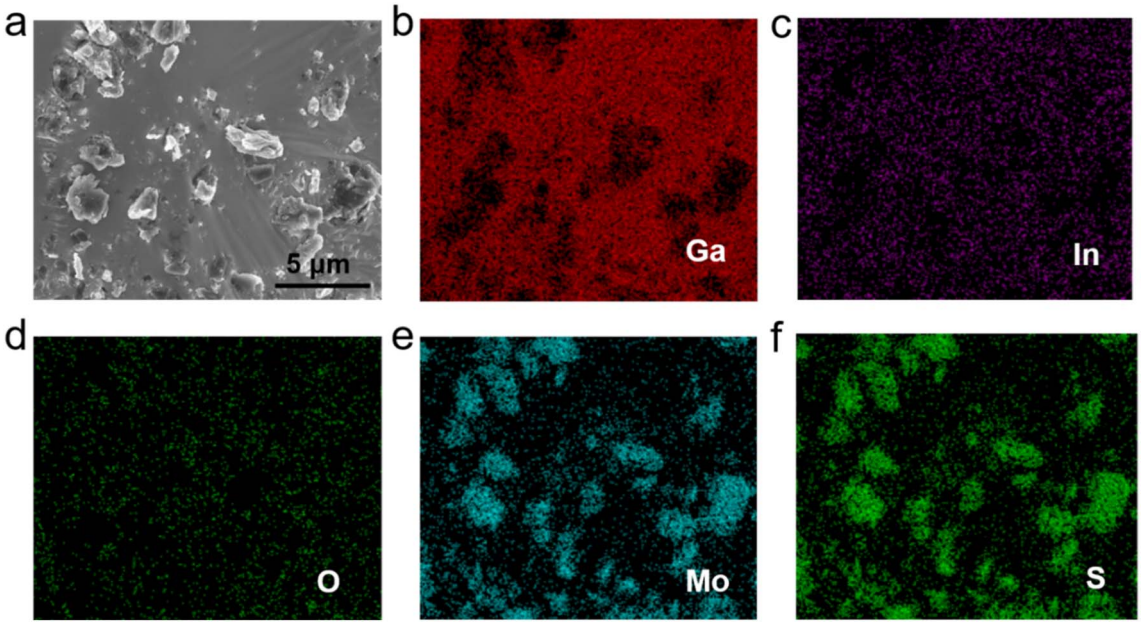

Fig. 4 (a) SEM image and (b)–(f) EDS elemental mappings of GLM@$5MoS_2$.

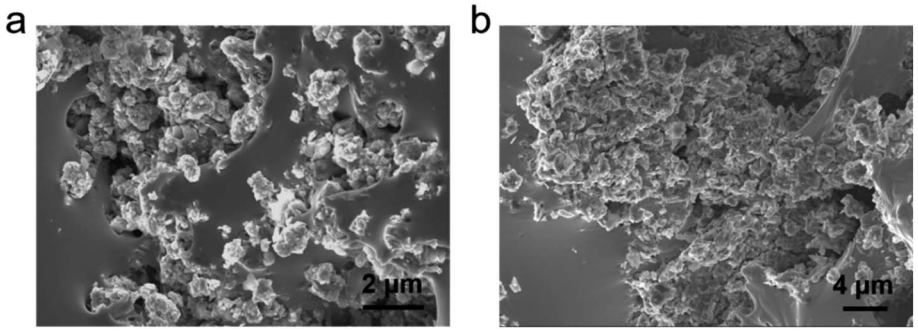

Fig. 5 SEM image of (a) GLM@12MoS_2 composite, (b) GLM@26MoS_2 composite.

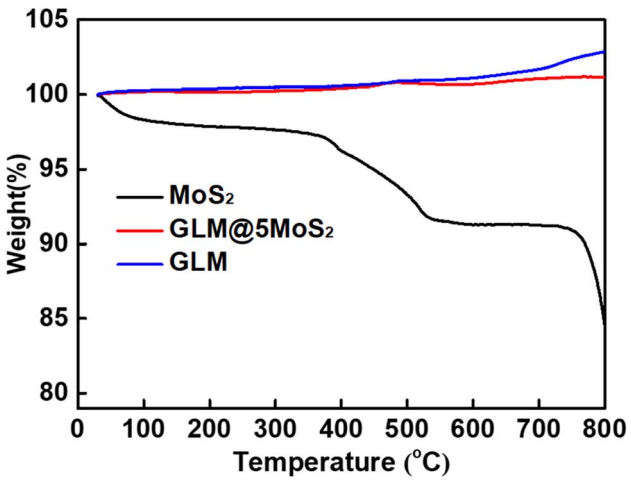

Fig. 6 The TGA curves of original MoS_2 nanosheets, pure GLM and prepared GLM@5MoS_2 composite.

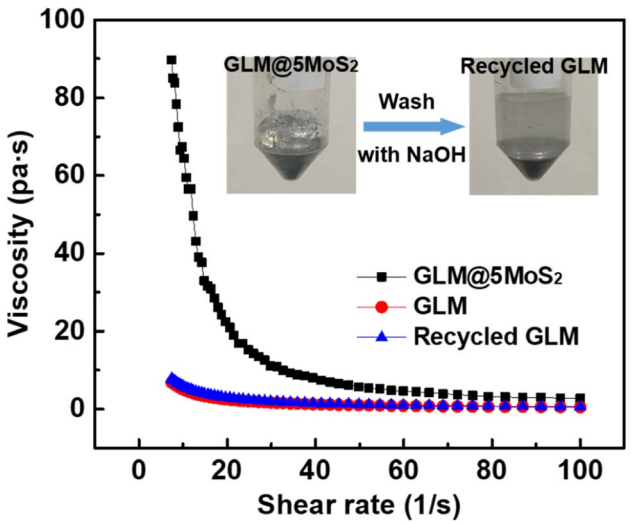

Fig. 7 The rheological characteristics of GLM@5MoS_2 composite, pure GLM and recycled GLM. The inset is the recycling process of GLM.

The morphology and chemical elements of GLM@5MoS_2 composite were characterized by SEM and EDS as shown in Fig. 4. It could be clearly seen from the results that MoS_2 nanosheets are embedded and well-dispersed in GLM matrix. The morphologies of GLM@12MoS_2 and GLM@26MoS_2 composites are demonstrated in Fig. 5. In comparison with GLM@5MoS_2 composite in Fig. 4, when the mass fraction of MoS_2 nanosheets reaches 12 wt% or 26 wt%, MoS_2 nanosheets in liquid metal are unable to be thoroughly dispersed and MoS_2 nanosheets progressively agglomerate into large particles.

The thermal property of prepared GLM@5MoS_2 composite was tested by thermo gravimetric analyser. TGA experimental results in Fig. 6 further confirm the integration between MoS_2 nanosheets and GLM. For MoS_2 nanosheets, the slight mass loss at the range of 100–780 °C is attributed to the removal of adsorptive hydrated H_2O and it shows an 8% weight loss before 780 °C. When the temperature is close to 800 °C, the MoS_2 nanosheets have a sudden weight loss due to the sublimation of MoS_2. For pure GLM, the curve generally demonstrates an upward trend, which is due to the oxidation of GLM and a slight increase in mass. In comparison, the GLM@5MoS_2 composite exhibits a less increase of weight because of the hybrid of MoS_2 nanosheets.

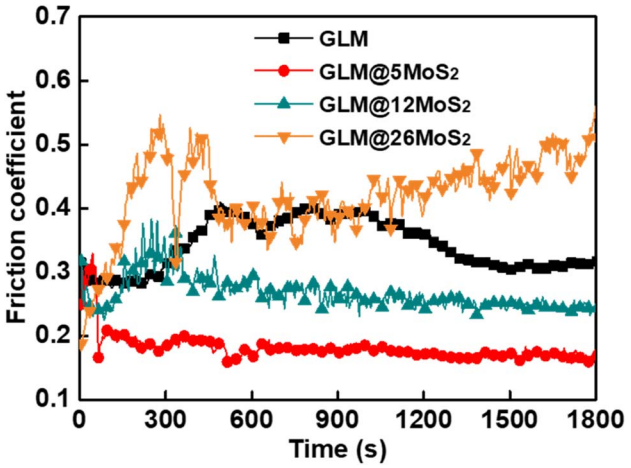

Fig. 8 Real-time friction coefficients lubricated by pure GLM, GLM@5MoS_2, GLM@12MoS_2, and GLM@26MoS_2 composite under the applied load of 25 N.

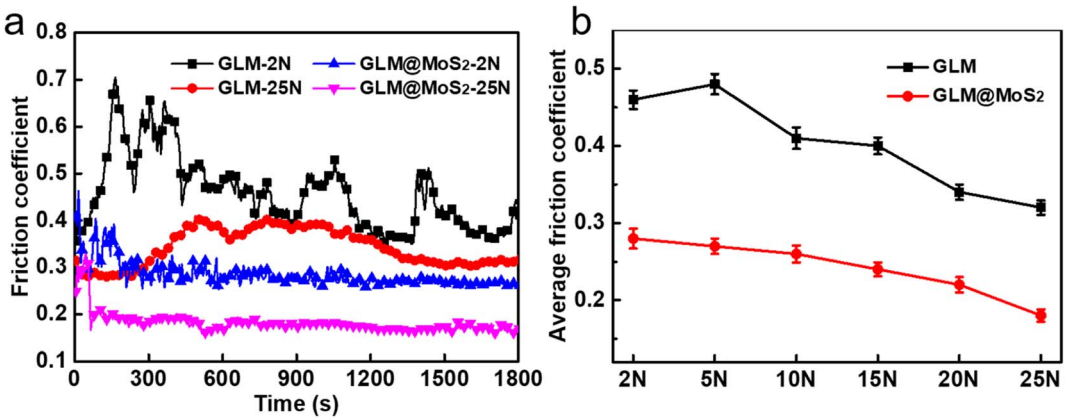

Fig. 9 (a) Comparison of real-time friction coefficient curves between pure GLM and GLM@5MoS_2 composite (b) average friction coefficients of pure GLM and GLM@5MoS_2 composite under different applied loads.

3.2 The reversible rheological property of GLM@MoS_2

There are two kinds of fillers in GLM: metallic and nonmetallic particles. In previous works, GLM based composite is commonly made by hybridizing metal particles into liquid metal, and the binding force between liquid metal and metal particles is derived from stable intermetallic chemical bonds.[32,33] Therefore, it is hard to recycle liquid metal from GLM based composite with metallic particles and the rheological property of this kind of composite is irreversible.

As for nonmetallic particles such as MoS_2 nanosheets in this study, they are hybridized into GLM by utilizing sticky layers of liquid metals' oxides. So, it is feasible to recycle GLM by dissolving liquid metals' oxides in alkali solution and the fabrication process of the composite is reversible. As demonstrated in Fig. 7, the obtained GLM@5MoS_2 composite holds reversible rheological property. The viscosity of GLM@5MoS_2 is decreased with the shear rate. GLM@5MoS_2 composite demonstrates the characteristic of non-Newtonian fluid, which could be ascribe to the addition of MoS_2 nanosheets. Whereas the original GLM and the recovered GLM exhibit the similar Newtonian property and the viscosities of them are almost consistent.

3.3 The tribological properties of GLM@MoS_2

Fig. 8 demonstrates the real-time friction coefficient curves lubricated by pure GLM and GLM@MoS_2 composites with different contents of MoS_2 nanosheets under the applied load of

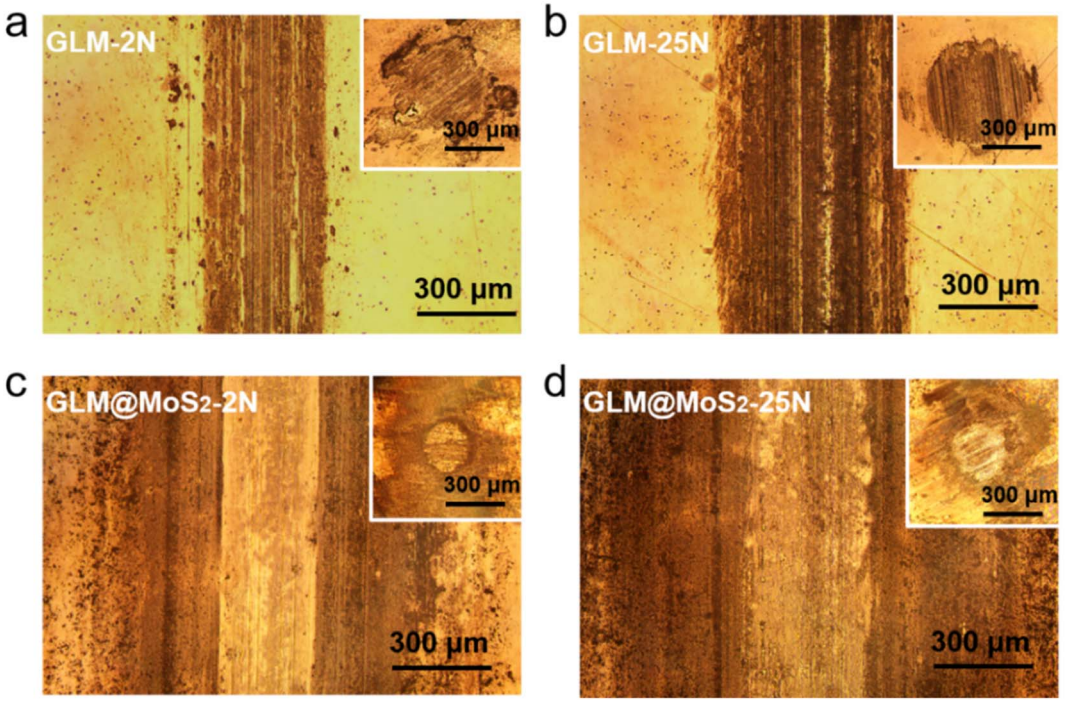

Fig. 10 OM images of wear tracks on the disks lubricated by (a) GLM under 2 N, (b) GLM under 25 N, (c) GLM@5MoS_2 composite under 2 N, (d) GLM@5MoS_2 composite under 25 N. The insets are corresponding wear scars on balls.

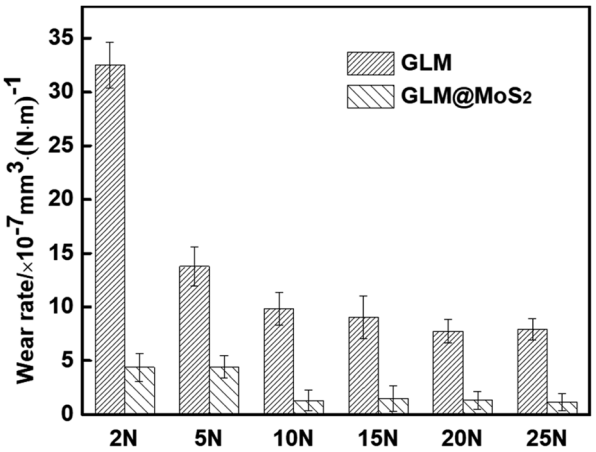

Fig. 11 Wear rates of GLM and GLM@5MoS_2 composite under different applied load conditions.

25 N. It could be concluded from the results in Fig. 8 that GLM@5MoS_2 holds the best anti-friction ability among all samples. The average friction coefficient of GLM@5MoS_2 is 0.18, which is 46% smaller than the friction coefficient of pure GLM. Since the pure MoS_2 is under solid state, the average friction coefficient of pure MoS_2 is as high as 0.72. With the increase of MoS_2 nanosheets in the GLM@MoS_2 composites, the anti-friction ability deteriorates. For GLM@26MoS_2 composite, the friction coefficient is even higher than pure GLM, which indicates the poor lubrication ability of GLM@26MoS_2 composite. We further investigated the lubrication ability of GLM@5MoS_2 composite under different applied loads and the results are shown in Fig. 9. The GLM@5MoS_2 composite holds better anti-friction ability than pure GLM under all experimental conditions and the GLM@5MoS_2 composite can exhibit better lubrication behaviour under high applied loads.

The worn conditions of disks and balls lubricated by pure GLM and GLM@5MoS_2 composite under applied loads of 2 N and 25 N are shown in Fig. 10. The average wear scar widths of different samples are marked in Fig. 10. It demonstrates that when GLM@5MoS_2 is utilized as lubricant, the wear scar tracks on disks and balls can be effectively reduced. And it is noticeable that the wear scar widths of GLM@5MoS_2 under loads of 2 N and 25 N are 247 μm and 330 μm respectively, which are smaller than that of pure GLM. Moreover, the wear rates on the steel balls are calculated based on eqn (1)–(3) and the results are shown in Fig. 11. The increase of applied load can reduce the wear rates of both pure GLM and GLM@5MoS_2 composite. Whereas GLM@5MoS_2 composite always holds lower wear rate value than that of pure GLM under all applied loads and the wear rate can be maximally reduced by 89% under the applied load of 2 N. Therefore, combined with friction coefficient curves, it can be concluded that GLM@5MoS_2 composite is conducive to improving anti-friction and anti-wear abilities of GLM matrix.

3.4 The lubrication mechanisms

For the sake of exploring the lubrication mechanisms of GLM@5MoS_2, SEM images and EDS analyses of worn surfaces

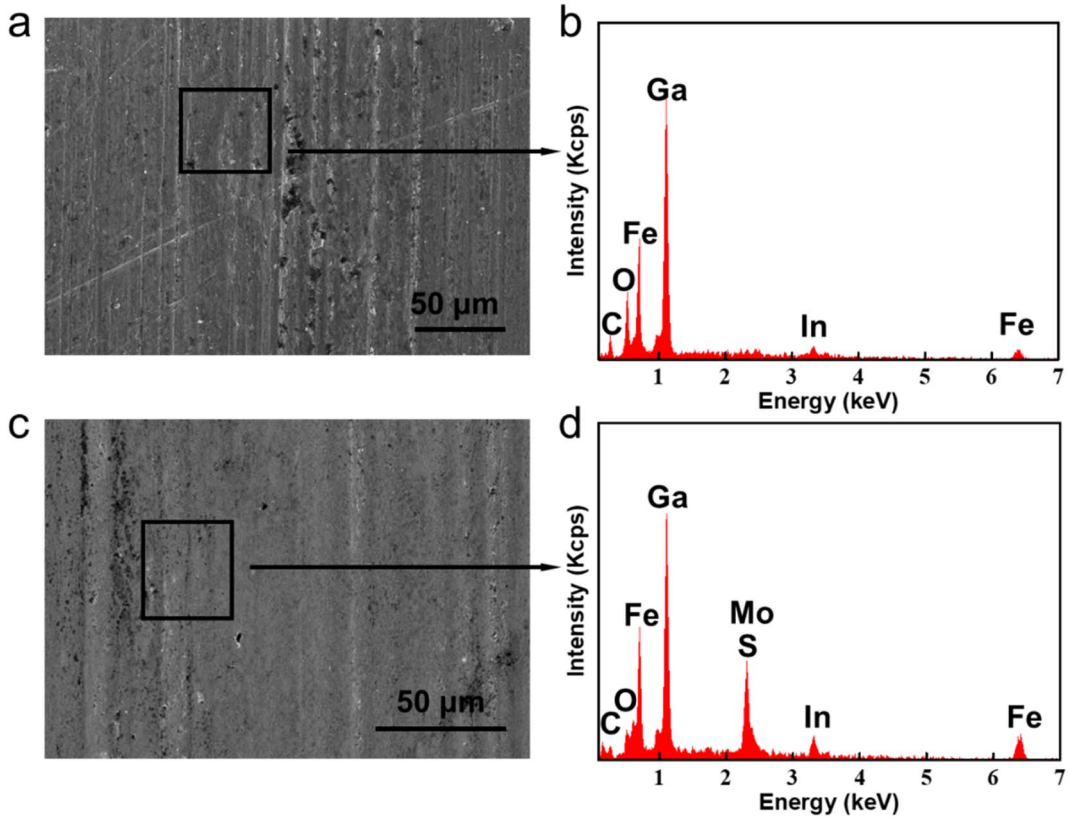

Fig. 12 SEM wear scar images and EDS analyses lubricated by (a) and (b) pure GLM, (c) and (d) GLM@5MoS_2 under 25 N.

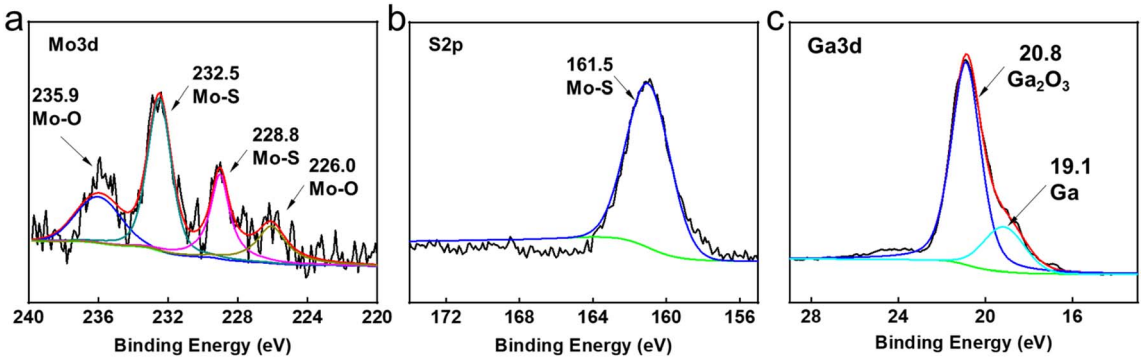

Fig. 13 High resolution XPS analyses of wear tracks lubricated by GLM@5MoS_2 under 25 N. (a) Mo3d, (b) S2p and (c) Ga3d.

are shown in Fig. 12. In comparison with the surface lubricated with pure GLM, less furrows are found on the surface lubricated by GLM@5MoS_2 composite. Combined with the EDS results, it could be concluded that there are some deposited tribo-films on the substrate, which are beneficial for improving lubrication abilities and mainly contain elements of Ga, Mo, S, O and In. To verify the chemical compositions of the tribo-films, XPS experiments are further carried out and the results are given in Fig. 13. The High resolution XPS analyses of Mo3d and Ga3d indicate the MoS_2 nanosheets and liquid gallium are oxidized slightly during the frictional process. Therefore, dominant compositions of tribo-films are Ga, MoS_2, and oxides of Ga and Mo.

4. Conclusions

In summary, this study proposed a facile grinding process to integrate MoS_2 into GLM, thus forming GLM@MoS_2 composite with reversible rheological properties and desirable lubrication abilities. Because the hybridization mechanisms of GLM@MoS_2 composite are attributed to sticky layers of liquid metals' oxides, it is feasible to recover GLM by dissolving liquid metals' oxides. And the recovered GLM exhibits the similar Newtonian property with the original GLM. The addition concentration of MoS_2 nanosheets shows prominent effect on the dispersion and lubrication abilities of GLM@MoS_2 composite. GLM@5MoS_2 and GLM@12MoS_2 composites are able to reduce the friction coefficient and wear rate of pure GLM, while the excessive addition of MoS_2 nanosheets deteriorates the lubrication condition due to agglomeration problem. Furthermore, the enhanced lubricity of GLM@MoS_2 composite could be ascribed to the deposited tribofilms between frictional pairs, which are composed of Ga, MoS_2, oxides of Ga and Mo. This study provided a feasible strategy to obtain GLM@MoS_2 composite with recoverable characteristic and enhanced lubrication ability, which could be expected to facilitate the application of GLM in lubrication and composite fields.

Conflicts of interest

The authors declare no conflict of interest.

Acknowledgements

This research is supported by Collaborative Innovation Center for Shangdong's Main crop Production Equipment and Mechanization (grant number SDXTZX-20). This work is also supported by the Qilu Youth Scholar Funding of Shandong University (31380082263065).

References

1 N. Kazem, T. Hellebrekers and C. Majidi, *Adv. Mater.*, 2017, **29**, 1605985.
2 E. J. Markvicka, M. D. Bartlett, X. Huang and C. Majidi, *Nat. Mater.*, 2018, **17**, 618–624.
3 T. V. Neumann, E. G. Facchine, B. Leonardo, S. Khan and M. D. Dickey, *Soft Matter*, 2020, **16**, 6608–6618.
4 M. H. Malakooti, M. R. Bockstaller, K. Matyjaszewski and C. Majidi, *Nanoscale Adv.*, 2020, **2**, 2668–2677.
5 H. Li, P. Tian, H. Lu, W. Jia, H. Du, X. Zhang, Q. Li and Y. Tian, *ACS Appl. Mater. Interfaces*, 2017, **9**, 5638–5644.
6 J. Cheng, Y. Yu, J. Guo, S. Wang, S. Zhu, Q. Ye, J. Yang and W. Liu, *Tribol. Int.*, 2019, **129**, 1–4.
7 J. Guo, J. Cheng, H. Tan, S. Zhu, Z. Qiao, J. Yang and W. Liu, *Tribol. Int.*, 2019, **135**, 457–462.
8 Y. Li, S. Zhang, Q. Ding, D. Feng, B. Qin and L. Hu, *Mater. Lett.*, 2018, **215**, 140–143.
9 P. Bai, S. Li, D. Tao, W. Jia, Y. Meng and Y. Tian, *Tribol. Int.*, 2018, **128**, 181–189.
10 P. Bai, S. Li, W. Jia, L. Ma, Y. Meng and Y. Tian, *Tribol. Int.*, 2020, **141**, 105904.
11 X. Li, Y. Li, Z. Tong, Q. Ma, Y. Ni and G. Dong, *Tribol. Int.*, 2019, **129**, 407–415.
12 J. Guo, J. Cheng, H. Tan, S. Zhu, Z. Qiao, J. Yang and W. Liu, *Langmuir*, 2019, **35**, 6905–6915.
13 J. Ma, C. Liu, W. Chen, J. Chen, Q. Li, J. Guo and J. Cheng, *Tribol. Int.*, 2022, **171**, 107520.
14 J. Tang, X. Zhao, J. Li, Y. Zhou and J. Liu, *Adv. Sci.*, 2017, **4**, 1700024.
15 F. Carle, K. Bai, J. Casara, K. Vanderlick and E. Brown, *Phys. Rev. Fluids*, 2017, **2**, 013301.
16 J. Tang, X. Zhao, J. Li, R. Guo, Y. Zhou and J. Liu, *ACS Appl. Mater. Interfaces*, 2017, **9**, 35977–35987.

17 H. Chang, R. Guo, Z. Sun, H. Wang, Y. Hou, Q. Wang, W. Rao and J. Liu, *Adv. Mater. Interfaces*, 2018, **5**, 1800571.
18 H. Chang, P. Zhang, R. Guo, Y. Cui, Y. Hou, Z. Sun and W. Rao, *ACS Appl. Mater. Interfaces*, 2020, **12**, 14125–14135.
19 W. Kong, Z. Wang, M. Wang, K. C. Manning, A. Uppal, M. D. Green, R. Y. Wang and K. Rykaczewski, *Adv. Mater.*, 2019, **31**, 1904309.
20 C. Hu, C. Yi, M. Bai, J. Lv and D. Tang, *RSC Adv.*, 2020, **10**, 17418–17426.
21 Y. Shi, J. Zhang, J. Pu, S. Ren, H. Wang, X. Fan, T. Ma and L. Wang, *Composites, Part B*, 2023, **250**, 110460.
22 S. Wenlong, D. Jianxin, Z. Hui, Y. Pei, Z. Jun and A. Xing, *J. Manuf. Process*, 2011, **13**, 8–15.
23 S. Mahathanabodee, T. Palathai, S. Raadnui, R. Tongsri and N. Sombatsompop, *Wear*, 2014, **316**, 37–48.
24 Y. Meng, J. Sun, J. He, F. Yang and P. Wu, *Colloids Surf., A*, 2021, **626**, 126999.
25 Z. Chen, M. Zhang, Z. Guo, H. Chen, H. Yan, F. Ren, Y. Jin, Z. Sun and P. Ren, *Composites, Part B*, 2023, **248**, 110374.
26 Y. Wang, Y. Du, J. Deng and Z. Wang, *Colloids Surf., A*, 2019, **562**, 321–328.
27 S. V. Prabhakar Vattikuti, C. Byon, C. Venkata Reddy, B. Venkatesh and J. Shim, *J. Mater. Sci.*, 2015, **50**, 5024–5038.
28 C. P. Koshy, P. K. Rajendrakumar and M. V. Thottackkad, *Wear*, 2015, **330–331**, 288–308.
29 Z. Chen, H. Yan, T. Liu and S. Niu, *Compos. Sci. Technol.*, 2016, **125**, 47–54.
30 M. J. Assael, I. J. Armyra, J. Brillo, S. V. Stankus, J. Wu and W. A. Wakeham, *J. Phys. Chem. Ref. Data*, 2012, **41**, 285.
31 M. Yunusa, G. J. Amador, D. M. Drotlef and M. Sitti, *Nano Lett.*, 2018, **18**, 2498–2504.
32 R. Guo, B. Cui, X. Zhao, M. Duan, X. Sun, R. Zhao, L. Sheng, J. Liu and J. Lu, *Mater. Horiz.*, 2020, **7**, 1845–1853.
33 X. Wang, W. Yao, R. Guo, X. Yang, J. Tang, J. Zhang, W. Gao, V. Timchenko and J. Liu, *Adv. Healthcare Mater.*, 2018, **7**, 1800318.